Cell Reports
Physical Science

CellPress
OPEN ACCESS

Article

Engineered Porous Nanocomposites That Deliver Remarkably Low Carbon Capture Energy Costs

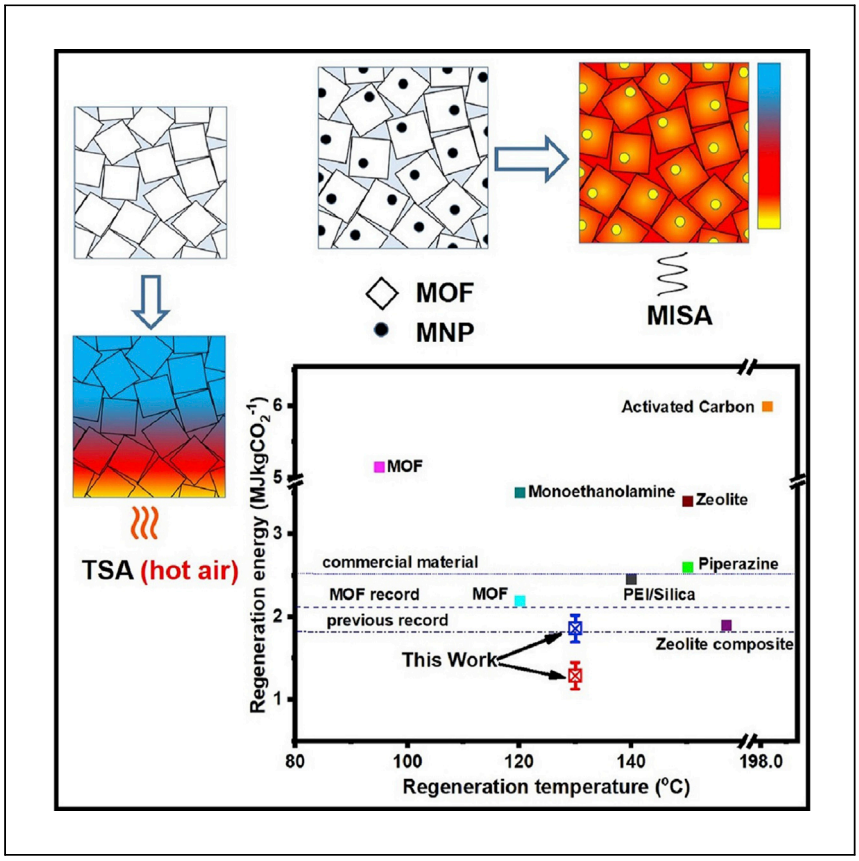

Sadiq et al. report a magnetic induction swing adsorption process with notable energy efficiency for the capture and release of CO_2. Incorporation of $MgFe_2O_4$ nanoparticles within Mg-MOF-74 allowed the CO_2 to have its release triggered by magnetic induction heating, requiring only 1.29 MJ kg^{-1}_{CO2}.

Muhammad Munir Sadiq, Kristina Konstas, Paolo Falcaro, Anita J. Hill, Kiyonori Suzuki, Matthew R. Hill

muhammad.sadiq@monash.edu (M.M.S.)
matthew.hill@csiro.au (M.R.H.)

HIGHLIGHTS

A magnetic induction swing adsorption (MISA) process for energy-efficient CO_2 capture

Remote, rapid, and localized heat generation in magnetic framework composites (MFCs)

<6 W electric power is required to drive MISA for CO_2 desorption from MFCs

The process resulted in high CO_2 productivity and adsorbent stability over multiple cycles

Sadiq et al., Cell Reports Physical Science *1*, 100070

https://doi.org/10.1016/j.xcrp.2020.100070

Cell Reports
Physical Science

CellPress
OPEN ACCESS

Article

Engineered Porous Nanocomposites That Deliver Remarkably Low Carbon Capture Energy Costs

Muhammad Munir Sadiq,[1,*] Kristina Konstas,[2] Paolo Falcaro,[3] Anita J. Hill,[2] Kiyonori Suzuki,[4] and Matthew R. Hill[1,2,5,*]

SUMMARY

A key barrier to the use of carbon dioxide capture technologies is the operating energy requirement, the chief contributor being the energy required to regenerate the capture media. When paired with electricity generation, the parasitic energy load can prohibit implementation. While metal organic frameworks (MOFs) harbor significant adsorption capacities, their thermally insulating nature will require significant energy and time to regenerate. Here, we report a MOF nanocomposite that can be regenerated at high speed and low energy cost. An adsorption system is tailored to deliver a very low energy cost of only 1.29 MJ kg^{-1}_{CO2}, 45% below commercially deployed materials, which can be exploited to deliver a productivity as high as 3.13 kg_{CO2} h^{-1} kg_{Ads}^{-1}. The combination of a MOF (Mg-MOF-74) with high adsorption capacity, a magnetic nanoparticle ($MgFe_2O_4$), and a porous hydrophobic polymer results in a composite that can be used in the magnetic induction swing adsorption (MISA) process.

INTRODUCTION

Global concerns about the rising level of greenhouse gas emissions and the associated environmental impact have led to renewed calls for emissions reduction and the development of green and renewable alternative energy sources.[1,2]

Post-combustion carbon capture and storage (CCS) has been proposed as a potential short-term solution that will significantly contribute to reducing global greenhouse gas emissions.[3-5] Existing commercial carbon capture technologies use amines such as monoethanolamine (MEA). The corrosive nature of MEA[6] and high energy requirements[2,7-11] associated with regeneration have limited the widescale deployment of CCS. Porous adsorbents such as zeolites and activated carbon are potential alternatives to amines.[12] However, these adsorbents require relatively high thermal regeneration conditions and have moderate CO_2 uptake and working capacities, which have limited their widespread deployment for CCS.[13,14]

Metal organic frameworks (MOFs) are crystalline porous adsorbents with an exceptional capacity to store guest molecules.[15-18] As such, they have been explored as adsorbents for CO_2 separation and storage.[14,19-22] Although they show a remarkable capacity to store small molecules, the thermally insulating nature of MOFs[23] and the relatively strong adsorption interactions with guest molecules leads to difficulty in recovering adsorbed molecules. For MOFs to gain widespread deployment for CCS applications, there is a need to minimize the energy input used in regeneration processes while maximizing the working capacity of the MOF.[24,25] The regeneration energy, which is the energy required to effect desorption in a typical

[1]Department of Chemical Engineering, Monash University, Clayton, 3168 VIC, Australia

[2]CSIRO Manufacturing, Private Bag 10, Clayton South MDC, 3169 VIC, Australia

[3]Graz University of Technology, Stremayrgasse 9/Z2, 8010 Graz, Austria

[4]Department of Materials Science and Engineering, Monash University, Clayton, 3168 VIC, Australia

[5]Lead Contact

*Correspondence: muhammad.sadiq@monash.edu (M.M.S.), matthew.hill@csiro.au (M.R.H.)

https://doi.org/10.1016/j.xcrp.2020.100070

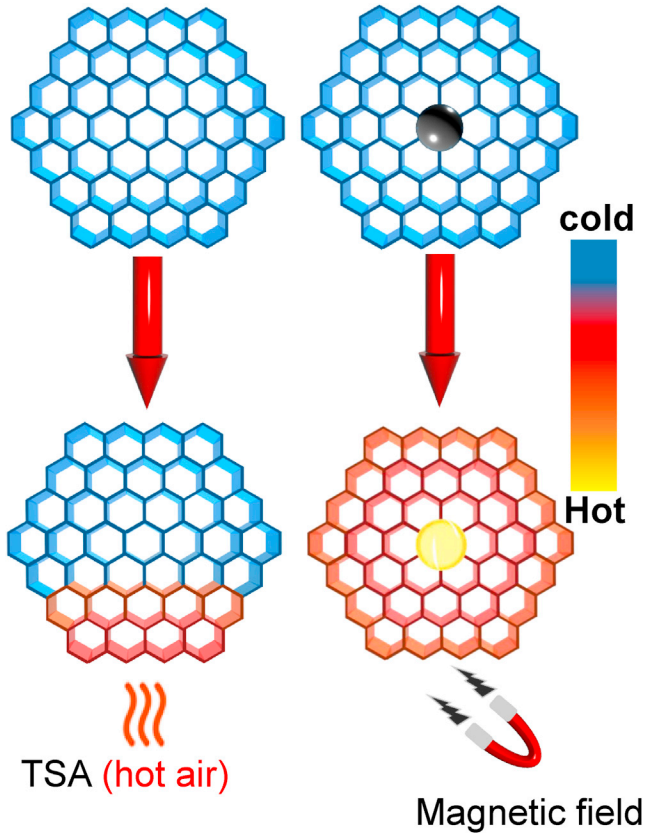

Figure 1. Comparison of Heat Transfer Mode between TSA and MISA in Adsorbents
The incorporation of magnetic nanoparticles in MOF adsorbents enables remote and rapid heat generation and transfer in MISA as compared to the gradual heat transfer process during regeneration in TSA processes.

adsorption-desorption process has been shown to lead to a high energy penalty when carbon capture is implemented for power plants and industrial processes.[26] A recent study indicated that MOFs may not yet possess the requisite efficiencies.[27]

Since MOFs are thermal insulators,[28] the heat transfer required for the temperature swing process can be inefficient. Thus, developing an effective regeneration process is key to deploying MOFs in CCS. A modified thermal swing adsorption (TSA) process[29] was reported, in which hot CO_2 was used as a purge gas for adsorbent regeneration, with up to 91% recovery of CO_2; however, this process required 3.4 MJ kg^{-1}_{CO2} at 150°C. In addition, electric swing adsorption was used on a zeolite-based composite for CO_2 post-combustion capture.[30] The process achieved a 72% recovery with a regeneration energy estimated at 1.9 MJ kg^{-1}_{CO2}, although there were questions regarding scalability.[30]

To this end, we have previously reported the proof of concept for using light,[3,31] magnetic fields,[32,33] and a combination of the two.[9] Here, we explore the optimized efficiency of the magnetic field process and investigate the stability and energy efficiency. Power losses from ferromagnetic and ferrimagnetic nanoparticles (NPs) embedded within a MOF, also called magnetic framework composites (MFCs),[34] are used for heat generation in a method known as magnetic induction swing adsorption (MISA).[32,33] Figure 1 shows a comparison of the slow and gradual heat

transfer in a typical TSA process in which hot air is used to regenerate the adsorbent as compared to the localized and rapid heating of the MISA process.

Unlike conventional heating methods, magnetic induction heating can deliver heat remotely to magnetic particles through a nonmagnetic insulating body, as successfully demonstrated in magnetic hyperthermia treatments.[35] Hence, it is a reasonable idea to incorporate finely dispersed magnetic particles in MOFs and thereby overcome their limited thermal diffusion length. However, our early-stage proof-of-concept composite works were limited to the milligram scale. The limited uptake capacity of the material and the limitation in our setup resulted in high regeneration energy for the composites. Thus, a proper evaluation of a high-capacity MOF composite is required to showcase the potential energy efficiency and cost savings that could be achieved with the MISA process.

We report a MISA study demonstrating a novel MFC comprising Mg-MOF-74, with a high concentration of coordinatively unsaturated metal sites and a high CO_2 capacity and selectivity at low pressures[36] and $MgFe_2O_4$ MNPs with high heating rates.[33,37] We explored two composite scenarios: (1) pre-synthesized MNPs embedded in Mg-MOF-74 by means of a 1-pot solvothermal strategy and (2) poly [1-(trimethylsilyl)-1-propyne] (PTMSP), a highly permeable polymer[38] used as a hydrophobic matrix to incorporate the MOFs and MNPs with the potential of slowing down the degradation of the MOF component in a humid environment.

RESULTS

Dynamic CO_2 Uptake and Release

Figure 2A is a pictorial representation of the homogeneous distribution of the MNPs in the M-74 composite (CPT) matrix. Scanning electron microscopy (SEM) analysis of M-74 CPT showed a rod-like morphology for the bare Mg-MOF-74 and M-74 CPT material (Figures 2B and 2C). Energy-dispersive X-ray (EDX) mapping microanalysis of M-74 CPT revealed a homogeneous distribution of the NPs, which is highlighted by the distribution of iron atoms in the MOF matrix (Figures 2C and 2D). Powder X-ray diffraction (PXRD) analysis of the composite materials demonstrates the retention of the pure phase pattern of bare MOF and MNP (Figure S1). The surface area of M-74 CPT, M-74 CPT@PTMSP, and bare MOF Mg-MOF-74 were measured (Figure S3) with N_2 at 77K and calculated using the Brunauer-Emmett-Teller (BET) theory, with determined surface areas of 1,200 $m^2\ g^{-1}$, 700 $m^2\ g^{-1}$, and 1,410 $m^2\ g^{-1}$, respectively.

CO_2 adsorption isotherms were collected at 298K (Figure S4). Mg-MOF-74 exhibited a CO_2 capacity of 8.72 mmol g^{-1}, while composites M-74 CPT and M-74 CPT@PTMSP displayed decreased CO_2 uptake of 6.69 mmol g^{-1} and 5.35 mmol g^{-1}, respectively, at 100 kPa. This represents a 23% and 39% decrease in CO_2 uptake relative to the bare Mg-MOF-74. This is ascribed to the effect of the non-porous NPs in the matrix of the MOF, yet it is notable that the CO_2 uptake decreases by less than the surface area, indicating a CO_2-philic surface.[39,40] The working capacities remain highly suited to post-combustion CO_2 capture.[41,42] The magnetic NP content of M-74 CPT was analyzed by comparing its saturation magnetization (M_s) with that of bare MNPs. M-74 CPT exhibited an M_s value of 16.6 A $m^2\ kg^{-1}$ relative to 73.5 A $m^2\ kg^{-1}$ for the as-synthesized MNPs (Figure S2). This represents ~23 wt% $MgFe_2O_4$ content in M-74 CPT. Comparatively, M-74 CPT@PTMSP exhibited an M_s value of 4.57 A m2 kg^{-1}, which represents 6 wt% $MgFe_2O_4$ content in M-74 CPT@PTMSP.

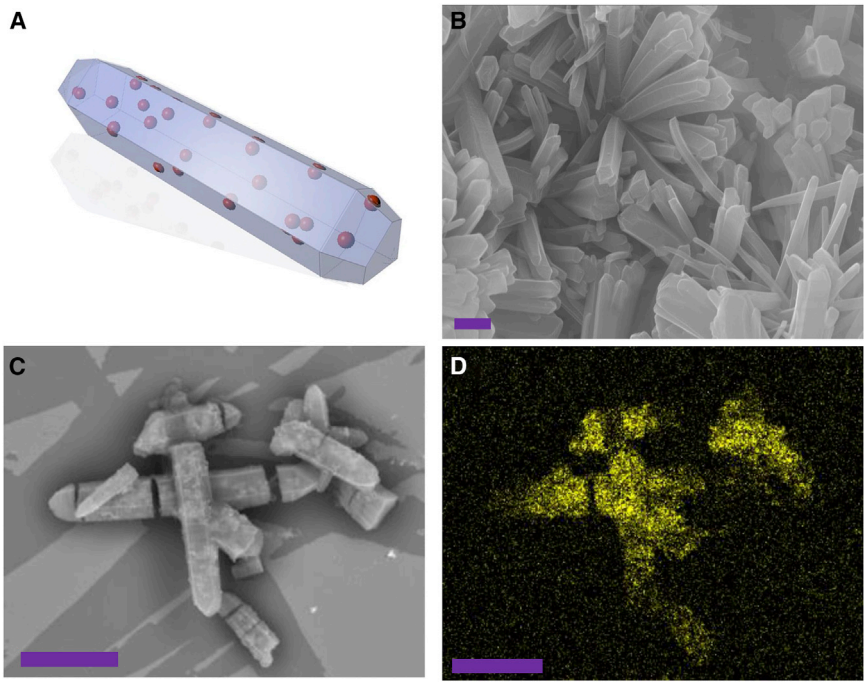

Figure 2. Morphology and Fe Mapping of Mg-MOF-74 and M-74 CPT

(A) Image depicting nanoparticle distribution in a MFC.

(B) SEM micrograph of bare Mg-MOF-74. Scale bar represents 1 μm.

(C) SEM micrograph of M-74 CPT. Scale bar represents 5 μm.

(D) Elemental mapping of Fe atoms in M-74 CPT. Scale bar represents 5 μm.

To evaluate the suitability of M-74 CPT for post-combustion CCS in a MISA process, it is important to establish the working capacity of the adsorbent at conditions similar to that of flue gas streams of power plants and industrial processes. The working capacity is estimated as the difference between the CO_2 uptake at 15 kPa (298K) and the CO_2 uptake at 100 kPa at different magnetic field-induced desorption temperatures (T_d).[2] Figure S6 shows the estimated working capacities for M-74 CPT obtained by recording the CO_2 magnetic isotherms (Figure S5) at different applied fields ($\mu_0 H$). Figure S5B shows the temperature increase profile under each applied magnetic field as recorded by an fiberoptic thermal sensor. A positive working capacity was attained at T_d = 80°C ($\mu_0 H$ = 15 mT) and 4.03 mmol g^{-1} (15.1 wt%) was achieved at $\mu_0 H$ = 21 mT corresponding to 145°C. This is marginally lower than that reported for bare Mg-MOF-74 (17.6 wt% at 200°C) in a TSA process.[2]

We attribute such high working capacities at relatively lower temperatures to the very fast and high heating rates that M-74 CPT attains when used in the MISA process. Dynamic triggered release experiments (Figure S17) for M-74 CPT at 21 mT and 15 kPa (Figure 3A) were performed over 10 cycles that resulted in an average of 85% CO_2 release efficiency per cycle. The remote and localized nature of the induction heating that leads to even heat distribution in the composite expectedly resulted in a low regeneration time of 7–11 min across the 10 cycles (Figure 3B). In practice, an important parameter that evaluates how frequent an adsorbent bed can be used in cyclic operations is known as "productivity," which is given by the amount of produced CO_2 per unit time and adsorbent mass.[29,43] The shorter the time to regenerate an adsorbent bed, the higher the productivity of the system,[43,44] and this leads to a larger production capacity.

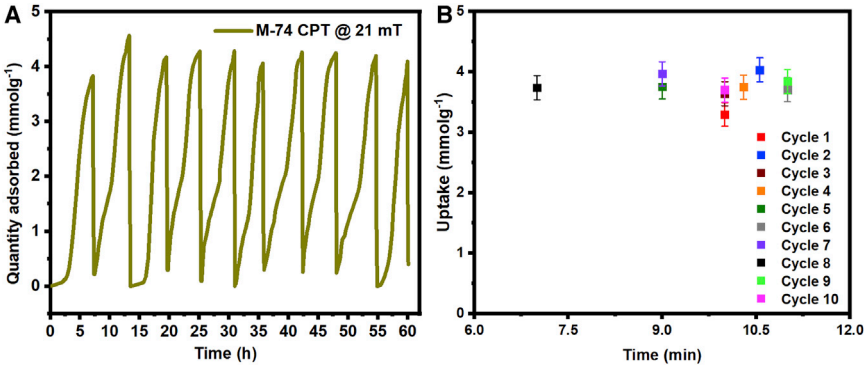

Figure 3. Performance Evaluation of M-74 CPT in the MISA Process

(A) Dynamic uptake and release of CO_2 from M-74 CPT@ 21 mT (145°C) and 0.15 kPa.

(B) Change in the amount of CO_2 desorbed as a function of time for M-74 CPT.

Error bar represents the standard deviation of CO_2 loading.

Breakthrough Experiments

MOFs have been shown to have properties that will make them suitable for a wide range of applications; however, a major limitation to their use is their instability in wet conditions.[45] Strategies to offset this have included post-synthetic modification with functional groups,[46] direct synthesis of stable MOFs,[47] and coating with polymeric materials to induce hydrophobicity.[42] These techniques are often tedious and involve difficult steps that could limit commercial-scale production of the material. For MOFs to be used in CCS applications, it is crucial to have materials that can be easily fabricated with relatively good stability and performance. As previously highlighted, the energy penalty associated with the use of porous adsorbents for CCS is governed significantly by the regeneration energy.[5,25] To evaluate the regeneration energy associated with deploying the MISA process with porous adsorbents, we modified the fabrication process of the composite by using PTMSP, a highly permeable hydrophobic polymer,[48] as a matrix for combining the MNPs with MOF to allow handling in ambient conditions and also slow down moisture uptake during breakthrough experiments. The stability of Mg-MOF-74@PTMSP was evaluated by exposing the composite to ambient conditions for 7 days. From Figure S4, it can be observed that relative to the bare Mg-MOF-74, which showed a 52% decrease in CO_2 uptake at room temperature and 15 kPa, Mg-MOF-74@PTMSP showed an only 8% decrease in performance, highlighting the contribution of PTMSP in slowing down the decomposition of the MOF in ambient conditions. The fabricated composite M-74 CPT@PTMSP was then used in breakthrough experiments using a rig with flow diagram shown in Figure S18. A total of 3 g M-74 CPT@PTMSP was packed into a bed with a height of 3.4 cm and a diameter of 1.5 cm. The volume of the bed was calculated to be 6 cm^3, resulting in a packing density of 0.5 g cm^{-3}. Breakthrough experiments (Figure S8) for a binary mixture of CO_2/N_2 in the post-combustion flue gas CO_2 partial pressure range (10%–15%)[49,50] at 100 and 200 standard cubic centimeters per minute (SCCM) were performed. Furthermore, wet feed conditions with H_2O concentrations of ~1.5% were evaluated to test the efficacy of the PTMSP polymer in slowing down the kinetics of H_2O uptake. The breakthrough experiments for the wet feed were carried out at the 10%–15% CO_2 partial pressure range, with feed flow rate increased to 230 SCCM.

Energy-Efficient MISA Regeneration

To assess the efficiency of our MISA process for post-combustion CCS, it is important to establish the regeneration energy of our composite material relative to other

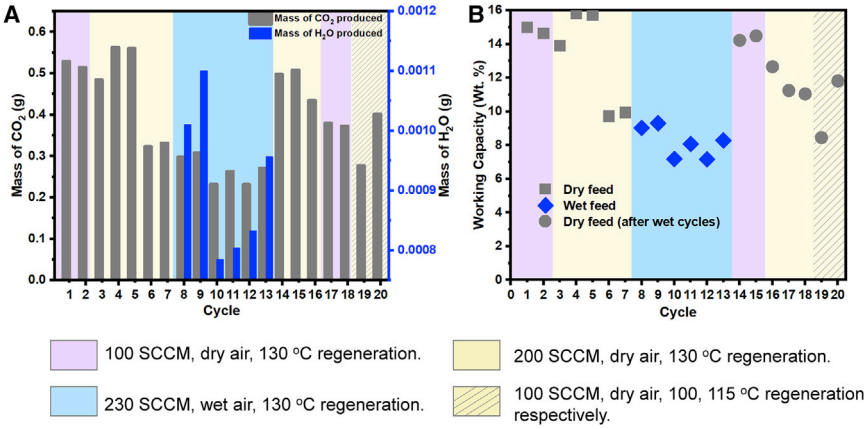

Figure 4. Performance Evaluation of M-74 CPT@PTMSP in the MISA Process

(A) Mass of CO_2 and H_2O recovered during MISA-induced regeneration of M-74 CPT@PTMSP.

(B) Working capacity of M-74 CPT@PTMSP over 20 cycles.

porous adsorbent materials. As highlighted earlier, PTMSP, a highly permeable polymer,[48] was used as a matrix to combine the MOF and MNP to increase the stability of the MOF and also induce resistance to water uptake by slowing down the kinetics of H_2O adsorption relative to CO_2. The performance of M-74 CPT@PTMSP was evaluated by estimating the amount of CO_2 and H_2O captured and desorbed via our MISA process over 20 consecutive cycles. By integrating the area under the breakthrough curves (Figure S9), the cumulative mass of CO_2 and H_2O produced during each cycle of the regeneration process is presented in Figures 4A, S10, and S11. The highest amount of CO_2 was produced during cycle 4, in which 0.56 g was generated for a 20°C adsorption temperature and a 130°C regeneration temperature. At an adsorption temperature of 40°C, similar to post-combustion flue gas temperatures, 0.38 g of CO_2 was produced (cycle 17). When H_2O was introduced to the feed, cycle 9, with an adsorption temperature of 20°C and a regeneration temperature of 130°C, 0.31 g of CO_2 was produced. Figure 4B presents the working capacity of M-74 CPT@PTMSP over 20 adsorption-regeneration cycles. This is calculated as the amount of CO_2 produced divided by the sum of the CO_2 produced and the mass of the adsorbent. The working capacity was evaluated based on adsorption and regeneration conditions for each run (see Table S1 for experimental conditions). M-74 CPT@PTMSP achieved a working capacity of 16 wt% for dry feed with a CO_2:N_2 of 14:86 and an adsorption temperature of 20°C (cycles 4 and 5). When the adsorption temperature was increased to 40°C, the working capacity dropped to 10 wt%, irrespective of the feed flow rate used (cycles 6 and 7). This is to be expected due to the exothermic nature of the adsorption process,[51] which will lead to a decrease in the amount of CO_2 adsorbed when the adsorption temperature is increased from 20°C to 40°C. However, in comparison to the reported performance for bare Mg-MOF-74 in using a vacuum desorption step, in which a bed temperature swing of 25°C was observed due to the high adsorption enthalpy,[27] our composite system recorded a bed temperature swing of only −7°C for both dry and wet feed conditions (Figure S13). We attribute this to the presence of the MNPs in the composite, which serve as a sink for the heat released during the adsorption process. Furthermore, Mg-MOF-74 has a thermal conductivity[52] of 0.3 W m^{-1} K^{-1}, making it more of an insulator. The higher thermal conductivity (4–14 W m^{-1} K^{-1})[53] of MNPs in the MFC improves the overall thermal conductivity of the MFC. In general, we envisage that using MNPs with higher thermal conductivity and MOFs with lower enthalpy of adsorption will significantly minimize the impact

of bed temperature swing during the adsorption process with porous materials. Cycles 8–13 were carried out by introducing up to 1.5% H_2O in the feed to evaluate whether there would be any impact on the performance of M-74 CPT@PTMSP for post-combustion CCS. From Figure 4A, the highest decrease in mass of CO_2 produced was observed in cycles 10 and 12, in which an −60% decrease was observed from the 0.56 g produced in cycle 4. Consequently, the working capacity for cycles 8–13 decreased to an average of 8 wt% over the 6 cycles. The effect of humid conditions on the structure and CO_2 uptake capacity of Mg-MOF 74 has been well documented.[45,54] Water vapor has also been reported to decrease the permeability of gases in pure PTMSP membranes.[55] It is important to establish the effect, if any, of the moist feed on the performance of the M-74 CPT@PTMSP bed. To this effect, breakthrough experiments and regeneration cycles 14–20 were conducted to determine whether the MOF component lost its efficacy after 6 repeated cycles with moist feed in cycles 8–13. A working capacity of 14 wt% was calculated for cycles 14 and 15, when the adsorption stage was performed at 20°C, and when the adsorption temperature was increased to 40°C in cycle 17, the working capacity dropped to 11 wt%, similar to working capacities obtained at this temperature before exposure of the bed to the moist feed. PXRD analysis of M-74 CPT@PTMSP after 20 cycles (Figure S1) showed a slight reduction in the intensity of the peaks, with no change in the peak positions relative to that of the as-synthesized M-74 CPT@PTMSP and bare Mg-MOF-74. These results indicate that the nanocomposite PTMSP binder can stabilize the MOF particulate beyond what is conventionally reported. We also evaluated the impact of a reduction in regeneration temperature on the working capacity by using a field strength of 13 and 14 mT in cycles 19 and 20, corresponding to a regeneration temperature of 100°C and 115°C (Figure S13). The working capacity of M-74 CPT@PTMSP reduced to 8 and 12 wt%, respectively. Thus, these temperatures are not sufficient to induce the release of all of the adsorbed CO_2 in the composite. From CO_2 adsorption isotherms in Figure S4, a working capacity of 14.5 wt% can be achieved for M-74 CPT@PTMSP at the appropriate regeneration conditions.

By monitoring the power generated in the induction coil and comparing it with the amount of energy generated by M-74 CPT for each regeneration cycle, calculations based on the specific absorption rate (SAR) of the MNPs (Figure S15) showed that energy conversion efficiencies of −75% can be reached at scale when this MOF is deployed for post-combustion CCS. This is in agreement with our previous work for a UiO-66-based composite[33] and with efficiencies quoted for magnetic induction heating.[61,62] Figure 5A presents regeneration energy calculations as a function of temperature evaluated from the working capacities, enthalpy of adsorption, and heat capacity (Figure S14) of M-74 CPT@PTMSP in comparison to values reported in the literature for processes that involves a swing in temperature for regeneration of the adsorbent or absorbent.

The regeneration energy calculated for M-74 CPT@PTMSP is to the best of our knowledge the lowest reported for any solid porous adsorbent. At magnetic fields of 14 and 15 mT, the regeneration energy calculated for M-74 CPT was 1.29 and 1.44 MJ kg CO_2^{-1}. When compared to other adsorbent materials such as piperazine,[56] MEA,[11] and activated carbon,[60] the regeneration energy for our system is much lower. An increase in the regeneration energy to a value of 1.86 MJ kg CO_2^{-1} was observed when moisture was introduced to the feed; however, we attribute this to the potential for moisture to be trapped in between the different layers in the packed bed as a result of the polymer used. Figure S8B shows no real breakthrough for H_2O, suggesting that moisture is slowly and continuously trapped in

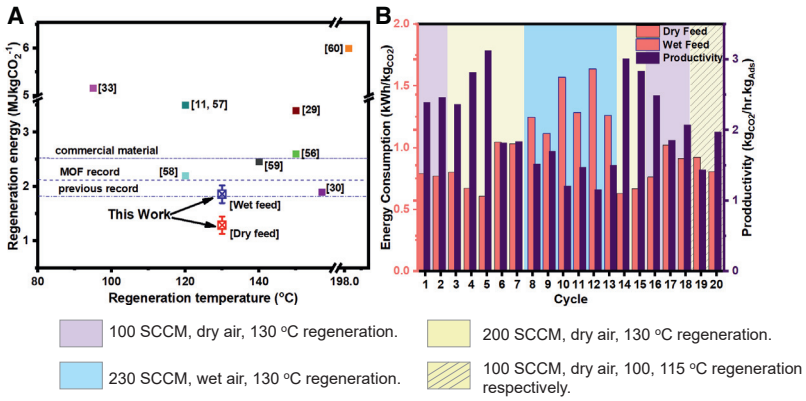

Figure 5. Evaluating the Efficiency of the MISA Process

(A) Regeneration energy as a function of desorption temperature for M-74 CPT in comparison to reported literature values. Piperazine,[56] monoethanolamine,[11,57] mmen-Mg-MOF-74,[58] polyethyleneimine (PEI)-silica,[59] activated carbon (AC) monolith,[60] UiO-66 MFC,[33] zeolite 13X,[30] and zeolite NaUSY.[29] Error bar represents standard deviation of calculated regeneration energies. (B) M-74 CPT@PTMSP energy consumption and productivity over 20 adsorption-desorption cycles. Energy consumption is estimated as the amount of electricity needed by the induction system to achieve the regeneration temperature.

the bed, thus leading to an −50% increase in the regeneration energy for the wet feed cycles. This tendency to trap moisture in the bed can be eliminated by deploying fluidized beds or having co-packing materials in the bed to minimize having layers of the MOF-polymer composite capable of trapping H_2O. As highlighted earlier, M-74 CPT@PTMSP retained its working capacity when dry feed was used post-wet feed cycles, confirming the efficacy of PTMSP in preventing moisture from getting to the MOF. M-74 CPT@PTMSP was completely regenerated using our MISA process, with regeneration temperatures within the range reported for other processes or materials; however, the regeneration energy required was much lower (1.29 MJ kg CO_2^{-1}). We attribute this to the extremely rapid and evenly distributed heating of the nanocomposite, resulting in a more efficient and effective release of adsorbed CO_2 molecules. We evaluated the efficiency of our MISA process by estimating the power used in driving the induction system at different magnetic field strengths. For desorption temperatures of 100°C, 115°C, and 130°C, corresponding to magnetic field strengths of 13, 14, and 15 mT, the power consumed by the sample was calculated as the difference between power consumed with and without the sample. From Figure S16, the power consumed at 13, 14, and 15 mT was estimated to be 4, 4.78, and 5.65 W, respectively.

Finally, and most significantly, we estimated the energy consumption for each cycle and compared it with the productivity of the M-74 CPT@PTMSP composite. The productivity is calculated as the working capacity divided by the time required for regeneration.[57] The productivity highlights the potential of our material deployed in the MISA process for post-combustion CCS. Figure 5B is a plot of the energy consumption and productivity over 20 cycles.

The lowest energy consumption for the composite was obtained in cycle 5 with 0.61 kWh/kg_{CO2} produced, with the highest value obtained in cycle 12 at 1.64 kWh/kg_{CO2}. This corresponds to the cycles with the highest and lowest amount of CO_2 produced. In addition, we also achieved very high productivity for M-74 CPT@PTMSP. In comparison to the productivity reported for bare Mg-MOF 74 (0.279 kg_{CO2} h^{-1} kg_{Ads}^{-1})[63] and commercial activated carbon

($0.08\ kg_{CO2}\ h^{-1}\ kg_{Ads}^{-1}$)[64] in TSA and temperature/vacuum swing adsorption (TVSA), respectively, M-74 CPT@PTMSP achieved a high productivity of $3.13\ kg_{CO2}\ h^{-1}\ kg_{Ads}^{-1}$ (dry feed) in cycle 5 and the lowest productivity of $1.16\ kg_{CO2}\ h^{-1}\ kg_{Ads}^{-1}$ (wet feed) in cycle 12. The purity of CO_2 produced via our process ranges from 21%–81% across the 20 cycles (Figure S12). The lowest purity was recorded when there was some H_2O in the feed gas used for the adsorption phase. In contrast to other thermal regeneration processes in which hot purge gas is used to regenerate the spent adsorbent, our MISA process will not incur the cost of heating up the purge gas with the potential of improving efficiency and purity by using minimal vacuum for product recovery.

DISCUSSION

The foregoing results have demonstrated the potential of the MISA process in significantly minimizing the energy penalty associated with post-combustion CCS with the use of solid porous adsorbents. Mg-MOF-74, a MOF with a very high working capacity was embedded with $MgFe_2O_4$ NPs having high heating rates (SAR) to make a composite. Due to the presence of the NPs, the composite showed a slightly lower CO_2 uptake capacity as compared to the bare MOF. Despite the decrease in CO_2 uptake, magnetically induced isotherms and dynamic release experiments for M-74 CPT showed very good working capacity and up to 80% release efficiency with conditions similar to that of flue gas from power plants and process industries. Breakthrough experiments and regeneration energy calculations from the MISA process resulted in a remarkable $1.29\ MJ\ kg_{CO2}^{-1}$ corresponding to a desorption temperature of 130°C for M-74 CPT@PTMSP. This is the lowest value reported so far for any porous solid adsorbent evaluated for post-combustion CCS. The composite also achieved a productivity of $3.13\ kg_{CO2}\ h^{-1}\ kg_{Ads}^{-1}$, with relatively small energy consumption required for heat generation during the regeneration phase. In addition, the introduction of PTMSP as a barrier to limit the effect of a humid environment on the composite proved crucial, as M-74 CPT@PTMSP retained working capacities similar to values obtained before introducing the wet feed. Thus, for CCS applications, incorporating porous hydrophobic polymers with MFCs is a viable route of fast tracking the adoption of MOFs for energy-efficient capture and separation.

EXPERIMENTAL PROCEDURES

Resource Availability

Lead Contact

Further information and requests for resources and procedures should be directed to the Lead Contact, A/Prof Matthew R. Hill (matthew.hill@csiro.au).

Materials Availability

This study did not generate new unique reagents.

Data and Code Availability

All of the data supporting the findings of this study are presented within the article and Supplemental Information. All other data are available from the Lead Contact upon reasonable request.

Magnetic Framework Composite Synthesis

In a typical process for composite fabrication (scenario 1), 0.472 g (2.4 mmol) of 2,5-dihydroxy-1,4-benzenedicarboxylic acid (DOBDC) and 1.96 g (8 mmol) of $Mg(NO_3)_2 \cdot 6H_2O$ were dissolved in 200 mL of a 14:1:1 (v/v/v) mixture of DMF (dimethylformamide)-ethanol-H_2O. The mixture was transferred to a round-bottom flask (RBF) containing 100 mg MNPs. The RBF was then fitted with a condenser and

mechanical stirrer. The reaction was carried out under a low argon flowrate, with the RBF placed in a dry heating bath at 130°C and 300 rpm for 15 h. After the reaction, the sample was cooled to room temperature. The mother solution was decanted and replaced with methanol. The composite was collected with a magnet and methanol was then decanted and replenished 4 times over 48 h. For the PTMSP-based composite (scenario 2), pre-synthesized Mg-MOF-74 (1 g) and MNPs (70 mg) were mixed in a 4-wt% PTMSP chloroform solution. The coating process produced a matrix of PTMSP-coated MOF and MNPs (see Figure S7). We call the resulting composites M-74 CPT and M-74 CPT@PTMSP, respectively. Further experimental details on magnetic MNP synthesis, breakthrough experimental procedure, and setup can be found in Methods S1.

SUPPLEMENTAL INFORMATION

Supplemental Information can be found online at https://doi.org/10.1016/j.xcrp.2020.100070.

ACKNOWLEDGMENTS

The authors acknowledge the use of facilities within the Monash Centre for Electron Microscopy and the Monash X-ray platform. Partial funding support was received from DP 180101023. M.R.H. acknowledges the Australian Research Council (ARC) for support (FT130100345).

AUTHOR CONTRIBUTIONS

Conceptualization, M.M.S., K.S., and M.R.H.; Methodology, M.M.S., K.K., K.S., and M.R.H.; Investigation, M.M.S., K.K., K.S., and M.R.H.; Writing – Original Draft, M.M.S.; Writing – Review & Editing, M.M.S., K.K., P.F., A.J.H., K.S., and M.R.H.; Funding Acquisition, K.S. and M.R.H.; Project Administration, M.M.S.; Resources, K.K., P.F., A.J.H., K.S., and M.R.H.; Supervision, K.S., A.J.H., P.F., and M.R.H.

DECLARATION OF INTERESTS

The authors declare no competing interests.

Received: January 29, 2020
Revised: March 6, 2020
Accepted: April 20, 2020
Published: June 4, 2020

REFERENCES

1. D'Alessandro, D.M., Smit, B., and Long, J.R. (2010). Carbon dioxide capture: prospects for new materials. Angew. Chem. Int. Ed. Engl *49*, 6058–6082.

2. Mason, J.A., Sumida, K., Herm, Z.R., Krishna, R., and Long, J.R. (2011). Evaluating metal-organic frameworks for post-combustion carbon dioxide capture via temperature swing adsorption. Energy Environ. Sci. *4*, 3030–3040.

3. Lyndon, R., Konstas, K., Ladewig, B.P., Southon, P.D., Kepert, P.C., and Hill, M.R. (2013). Dynamic photo-switching in metal-organic frameworks as a route to low-energy carbon dioxide capture and release. Angew. Chem. Int. Ed. Engl. *52*, 3695–3698.

4. Liu, Y.Y., Wang, Z.Y.U., and Zhou, H.C. (2012). Recent advances in carbon dioxide capture with metal-organic frameworks. Greenh. Gases (Chichester UK) *2*, 239–259.

5. Huck, J.M., Lin, L.C., Berger, A.H., Shahrak, M.N., Martin, R.L., Bhown, A.S., Haranczyk, M., Reuter, K., and Smit, B. (2014). Evaluating different classes of porous materials for carbon capture. Energy Environ. Sci. *7*, 4132–4146.

6. Fytianos, G., Grimstvedt, A., Knuutila, H., and Svendsen, H.F. (2014). Effect of MEA's degradation products on corrosion at CO2 capture plants. Enrgy Proced *63*, 1869–1875.

7. Simmons, J.M., Wu, H., Zhou, W., and Yildirim, T. (2011). Carbon capture in metal-organic frameworks-a comparative study. Energy Environ. Sci. *4*, 2177–2185.

8. Sumida, K., Rogow, D.L., Mason, J.A., McDonald, T.M., Bloch, E.D., Herm, Z.R., Bae, T.H., and Long, J.R. (2012). Carbon dioxide capture in metal-organic frameworks. Chem. Rev. *112*, 724–781.

9. Li, H.Q., Sadiq, M.M., Suzuki, K., Doblin, C., Lim, S., Falcaro, P., Hill, A.J., and Hill, M.R. (2016). MaLISA - a cooperative method to release adsorbed gases from metal-organic frameworks. J. Mater. Chem. A Mater. Energy Sustain. *4*, 18757–18762.

10. Markewitz, P., Kuckshinrichs, W., Leitner, W., Linssen, J., Zapp, P., Bongartz, R., Schreiber, A., and Muller, T.E. (2012). Worldwide innovations in the development of carbon capture technologies and the utilization of CO2. Energy Environ. Sci. *5*, 7281–7305.

11. Boot-Handford, M.E., Abanades, J.C., Anthony, E.J., Blunt, M.J., Brandani, S., Mac

Dowell, N., Fernandez, J.R., Ferrari, M.C., Gross, R., Hallett, J.P., et al. (2014). Carbon capture and storage update. Energy Environ. Sci. *7*, 130–189.

12. Hauchhum, L., and Mahanta, P. (2014). Carbon dioxide adsorption on zeolites and activated carbon by pressure swing adsorption in a fixed bed. Int. J. Energy Environ. Eng. *5*, 349–356.

13. Wang, J.Y., Huang, L., Yang, R.Y., Zhang, Z., Wu, J.W., Gao, Y.S., Wang, Q., O'Hare, D., and Zhong, Z.Y. (2014). Recent advances in solid sorbents for CO2 capture and new development trends. Energy Environ. Sci. *7*, 3478–3518.

14. Zhang, Z.J., Yao, Z.Z., Xiang, S.C., and Chen, B.L. (2014). Perspective of microporous metal-organic frameworks for CO2 capture and separation. Energy Environ. Sci. *7*, 2868–2899.

15. Yaghi, O.M., O'Keeffe, M., Ockwig, N.W., Chae, H.K., Eddaoudi, M., and Kim, J. (2003). Reticular synthesis and the design of new materials. Nature *423*, 705–714.

16. Zhang, J.-P., and Chen, X.-M. (2014). Metal-Organic Frameworks for Photonics Applications, *Volume 157, Chapter 100*, B. Chen and G. Qian, eds. (Springer Berlin Heidelberg), pp. 1–26.

17. Lee, W.R., Jo, H., Yang, L.M., Lee, H., Ryu, D.W., Lim, K.S., Song, J.H., Min, D.Y., Han, S.S., Seo, J.G., et al. (2015). Exceptional CO_2 working capacity in a heterodiamine-grafted metal-organic framework. Chem. Sci. (Camb.) *6*, 3697–3705.

18. Xiang, S., Zhou, W., Zhang, Z., Green, M.A., Liu, Y., and Chen, B. (2010). Open metal sites within isostructural metal-organic frameworks for differential recognition of acetylene and extraordinarily high acetylene storage capacity at room temperature. Angew. Chem. Int. Ed. Engl. *49*, 4615–4618.

19. Liao, P.Q., Zhou, D.D., Zhu, A.X., Jiang, L., Lin, R.B., Zhang, J.P., and Chen, X.M. (2012). Strong and dynamic CO2 sorption in a flexible porous framework possessing guest chelating claws. J. Am. Chem. Soc. *134*, 17380–17383.

20. Debatin, F., Thomas, A., Kelling, A., Hedin, N., Bacsik, Z., Senkovska, I., Kaskel, S., Junginger, M., Müller, H., Schilde, U., et al. (2010). In Situ Synthesis of an Imidazolate-4-amide-5-imidate Ligand and Formation of a Microporous Zinc-Organic Framework with H2-and CO2-Storage Ability. Angew. Chem. *122*, 1280–1284.

21. Thallapally, P.K., Tian, J., Radha Kishan, M., Fernandez, C.A., Dalgarno, S.J., McGrail, P.B., Warren, J.E., and Atwood, J.L. (2008). Flexible (breathing) interpenetrated metal-organic frameworks for CO2 separation applications. J. Am. Chem. Soc. *130*, 16842–16843.

22. Nandi, S., Collins, S., Chakraborty, D., Banerjee, D., Thallapally, P.K., Woo, T.K., and Vaidhyanathan, R. (2017). Ultralow Parasitic Energy for Postcombustion CO_2 Capture Realized in a Nickel Isonicotinate Metal-Organic Framework with Excellent Moisture Stability. J. Am. Chem. Soc. *139*, 1734–1737.

23. Huang, B.L., Ni, Z., Millward, A., McGaughey, A.J.H., Uher, C., Kaviany, M., and Yaghi, O. (2007). Thermal conductivity of a metal-organic framework (MOF-5): Part II. Measurement. Int. J. Heat Mass Transfer *50*, 405–411.

24. Berger, A.H., and Bhown, A.S. (2011). Comparing Physisorption and Chemisorption Solid Sorbents for use Separating CO2 from Flue Gas using Temperature Swing Adsorption. In 10th International Conference on Greenhouse Gas Control Technologies *4*, 562–567.

25. Lin, L.-C., Berger, A.H., Martin, R.L., Kim, J., Swisher, J.A., Jariwala, K., Rycroft, C.H., Bhown, A.S., Deem, M.W., Haranczyk, M., and Smit, B. (2012). In silico screening of carbon-capture materials. Nat. Mater. *11*, 633–641.

26. Lyndon, R., Konstas, K., Ladewig, B.P., Southon, P.D., Kepert, P.C.J., and Hill, M.R. (2013). Dynamic Photo-Switching in Metal–Organic Frameworks as a Route to Low-Energy Carbon Dioxide Capture and Release, Angewandte Chemie International Edition, 52, Angew. Chem, 2013, 3125, 3783-3786.

27. Danaci, D., Bui, M., Mac Dowell, N., and Petit, C. (2020). Exploring the limits of adsorption-based CO2 capture using MOFs with PVSA - from molecular design to process economics. Mol. Syst. Des. Eng. *5*, 212–231.

28. Sun, L., Liao, B.L., Sheberla, D., Kraemer, D., Zhou, J.W., Stach, E.A., Zakharov, D., Stavila, V., Talin, A.A., Ge, Y.C., et al. (2017). A Microporous and Naturally Nanostructured Thermoelectric Metal-Organic Framework with Ultralow Thermal Conductivity. Joule *1*, 168–177.

29. Ntiamoah, A., Ling, J.H., Xiao, P., Webley, P.A., and Zhai, Y.C. (2016). CO2 Capture by Temperature Swing Adsorption: Use of Hot CO2-Rich Gas for Regeneration. Ind. Eng. Chem. Res. *55*, 703–713.

30. Grande, C.A., Ribeiro, R.P.P.L., Oliveira, E.L.G., and Rodrigues, A.E. (2009). Electric swing adsorption as emerging CO2 capture technique. Greenhouse Gas Control Technologies *9*, 1219–1225.

31. Lyndon, R., Konstas, K., Thornton, A.W., Seeber, A.J., Ladewig, B.P., and Hill, M.R. (2015). Visible Light-Triggered Capture and Release of CO2 from Stable Metal Organic Frameworks. Chem. Mater. *27*, 7882–7888.

32. Li, H., Sadiq, M.M., Suzuki, K., Ricco, R., Doblin, C., Hill, A.J., Lim, S., Falcaro, P., and Hill, M.R. (2016). Magnetic Metal-Organic Frameworks for Efficient Carbon Dioxide Capture and Remote Trigger Release. Adv. Mater. *28*, 1839–1844.

33. Sadiq, M.M., Li, H., Hill, A.J., Falcaro, P., Hill, M.R., and Suzuki, K. (2016). Magnetic Induction Swing Adsorption: An Energy Efficient Route to Porous Adsorbent Regeneration. Chem. Mater. *28*, 6219–6226.

34. Ricco, R., Malfatti, L., Takahashi, M., Hill, A.J., and Falcaro, P. (2013). Applications of magnetic metal-organic framework composites. J. Mater. Chem. A Mater. Energy Sustain. *1*, 13033–13045.

35. Lu, A.H., Salabas, E.L., and Schüth, F. (2007). Magnetic nanoparticles: synthesis, protection, functionalization, and application. Angew. Chem. Int. Ed. Engl. *46*, 1222–1244.

36. Britt, D., Furukawa, H., Wang, B., Glover, T.G., and Yaghi, O.M. (2009). Highly efficient separation of carbon dioxide by a metal-organic framework replete with open metal sites. Proc. Natl. Acad. Sci. USA *106*, 20637–20640.

37. Yazaydin, A.O., Snurr, R.Q., Park, T.H., Koh, K., Liu, J., Levan, M.D., Benin, A.I., Jakubczak, P., Lanuza, M., Galloway, D.B., et al. (2009). Screening of metal-organic frameworks for carbon dioxide capture from flue gas using a combined experimental and modeling approach. J. Am. Chem. Soc. *131*, 18198–18199.

38. Bazhenov, S.D., Borisov, I.L., Bakhtin, D.S., Rybakova, A.N., Khotimskiy, V.S., Molchanov, S.P., and Volkov, V.V. (2016). High-permeance crosslinked PTMSP thin-film composite membranes as supports for CO2 selective layer formation. Green Energy Environ *1*, 235–245.

39. Lu, G., Li, S., Guo, Z., Farha, O.K., Hauser, B.G., Qi, X., Wang, Y., Wang, X., Han, S., Liu, X., et al. (2012). Imparting functionality to a metal-organic framework material by controlled nanoparticle encapsulation. Nat. Chem. *4*, 310–316.

40. Falcaro, P., Normandin, F., Takahashi, M., Scopece, P., Amenitsch, H., Costacurta, S., Doherty, C.M., Laird, J.S., Lay, M.D., Lisi, F., et al. (2011). Dynamic control of MOF-5 crystal positioning using a magnetic field. Adv. Mater. *23*, 3901–3906.

41. Xie, K., Fu, Q., Xu, C.L., Lu, H., Zhao, Q.H., Curtain, R., Gu, D.Y., Webley, P.A., and Qiao, G.G. (2018). Continuous assembly of a polymer on a metal-organic framework (CAP on MOF): a 30 nm thick polymeric gas separation membrane. Energy Environ. Sci. *11*, 544–550.

42. Zhang, W., Hu, Y., Ge, J., Jiang, H.L., and Yu, S.H. (2014). A facile and general coating approach to moisture/water-resistant metal-organic frameworks with intact porosity. J. Am. Chem. Soc. *136*, 16978–16981.

43. Joss, L., Gazzani, M., and Mazzotti, M. (2017). Rational design of temperature swing adsorption cycles for post-combustion CO2 capture. Chem. Eng. Sci. *158*, 381–394.

44. Luo, L. (2013). Chapter 2. In Heat and Mass Transfer Intensification and Shape Optimization, L. Luo, ed. (Springer London) 10.1007/978-1-4471-4742-8_2.

45. Zuluaga, S., Fuentes-Fernandez, E.M.A., Tan, K., Xu, F., Li, J., Chabal, Y.J., and Thonhauser, T. (2016). Understanding and controlling water stability of MOF-74. J. Mater. Chem. A Mater. Energy Sustain. *4*, 5176–5183.

46. Wang, Z., and Cohen, S.M. (2009). Postsynthetic modification of metal-organic frameworks. Chem. Soc. Rev. *38*, 1315–1329.

47. Feng, D., Chung, W.C., Wei, Z., Gu, Z.Y., Jiang, H.L., Chen, Y.P., Darensbourg, D.J., and Zhou, H.C. (2013). Construction of ultrastable porphyrin Zr metal-organic frameworks through linker elimination. J. Am. Chem. Soc. *135*, 17105–17110.

48. Cheng, X.Q., Konstas, K., Doherty, C.M., Wood, C.D., Mulet, X., Xie, Z., Ng, D., Hill, M.R., Shao, L., and Lau, C.H. (2017). Hyper-Cross-Linked Additives that Impede Aging and Enhance Permeability in Thin Polyacetylene Films for Organic Solvent Nanofiltration. ACS Appl. Mater. Interfaces *9*, 14401–14408.

49. Merel, J., Clausse, M., and Meunier, F. (2008). Experimental Investigation on CO2 Post−Combustion Capture by Indirect Thermal Swing Adsorption Using 13X and 5A Zeolites. Ind. Eng. Chem. Res. *47*, 209–215.

50. Liu, J., Tian, J., Thallapally, P.K., and McGrail, B.P. (2012). Selective CO2 Capture from Flue Gas Using Metal-Organic Frameworks-A Fixed Bed Study. J. Phys. Chem. C *116*, 9575–9581.

51. Su, F., Lu, C., and Chen, H.S. (2011). Adsorption, desorption, and thermodynamic studies of CO2 with high-amine-loaded multiwalled carbon nanotubes. Langmuir *27*, 8090–8098.

52. Qasem, N.A.A., and Ben-Mansour, R. (2018). Adsorption breakthrough and cycling stability of carbon dioxide separation from CO2/N2/H2O mixture under ambient conditions using 13X and Mg-MOF-74. Appl. Energy *230*, 1093–1107.

53. Maki, R.S.S., Mitani, S., and Mori, T. (2016). Effect of spark plasma sintering (SPS) on the thermoelectric properties of magnesium ferrite. Mater. Renew. Sustain. Energy *6*, 2.

54. DeCoste, J.B., Peterson, G.W., Schindler, B.J., Killops, K.L., Browe, M.A., and Mahle, J.J. (2013). The effect of water adsorption on the structure of the carboxylate containing metal-organic frameworks Cu-BTC, Mg-MOF-74, and UiO-66. J. Mater. Chem. A Mater. Energy Sustain. *1*, 11922–11932.

55. Fernandez-Barquin, A., Rea, R., Venturi, D., Giacinti-Baschetti, M., De Angelis, M.G., Casado-Coterillo, C., and Irabien, A. (2018). Effect of relative humidity on the gas transport properties of zeolite A/PTMSP mixed matrix membranes. Rsc Adv *8*, 3536–3546.

56. Rochelle, G., Chen, E., Freeman, S., Van Wagener, D., Xu, Q., and Voice, A. (2011). Aqueous piperazine as the new standard for CO2 capture technology. Chem. Eng. J. *171*, 725–733.

57. Abu-Zahra, M.R.M., Niederer, J.P.M., Feron, P.H.M., and Versteeg, G.F. (2007). CO2 capture from power plants - Part II. A parametric study of the economical performance based on mono-ethanolamine. Int. J. Greenh. Gas Control *1*, 135–142.

58. McDonald, T.M., Mason, J.A., Kong, X., Bloch, E.D., Gygi, D., Dani, A., Crocellà, V., Giordanino, F., Odoh, S.O., Drisdell, W.S., et al. (2015). Cooperative insertion of CO2 in diamine-appended metal-organic frameworks. Nature *519*, 303–308.

59. Zhang, W.B., Liu, H., Sun, Y., Cakstins, J., Sun, C.G., and Snape, C.E. (2016). Parametric study on the regeneration heat requirement of an amine-based solid adsorbent process for post-combustion carbon capture. Appl. Energy *168*, 394–405.

60. Grande, C.A., and Rodrigues, A.E. (2008). Electric Swing Adsorption for CO2 removal from flue gases. Int. J. Greenh. Gas Control *2*, 194–202.

61. Lucia, O., Acero, J., Carretero, C., and Burdio, J.M. (2013). Induction Heating Appliances Toward More Flexible Cooking Surfaces. Ieee Ind Electron M *7*, 35–47.

62. Kenneth, F., Mats, A., Tord, C., Leif, S., Peter, J., and Jan-Eric, S. presented in part at the 44th CIRP Conference on Manufacturing Systems Madison, 2011.

63. Ben-Mansour, R., and Qasem, N.A.A. (2018). An efficient temperature swing adsorption (TSA) process for separating CO2 from CO2/N2 mixture using Mg-MOF-74. Energy Convers. Manage. *156*, 10–24.

64. Plaza, M.G., García, S., Rubiera, F., Pis, J.J., and Pevida, C. (2010). Post-combustion CO2 capture with a commercial activated carbon: Comparison of different regeneration strategies. Chem. Eng. J. *163*, 41–47.